ELSEVIER

Materials Science and Engineering A333 (2002) 146–154

MATERIALS SCIENCE & ENGINEERING A

www.elsevier.com/locate/msea

Fracture criterion and forming pressure design for superplastic bulging

Li Chuan Chung, Jung-Ho Cheng *

Department of Mechanical Engineering, National Taiwan University, No. 1 Roosevelt Road, Section 4, Taipei 106, Taiwan, ROC

Received 13 July 2001; received in revised form 13 September 2001

Abstract

The flow localization factor (FLF), which enables quantitative description of the localization process of unstable plastic flow, was proposed in the authors' previous work. In this paper, the relation between the FLF and superplastic forming limits is further investigated via finite element simulations and experiments on the bulging of superplastic Ti–6Al–4V sheets at 900 °C. With the insight from these studies, a superplastic fracture criterion, which is in terms of an integral form of the FLF, is proposed. Fracturing is explained as the result when the flow localization accumulated throughout the entire forming process achieves a critical value. Satisfactory results are obtained for the verifications of the fracture criterion under various forming conditions. Finally, pressure design guidelines for superplastic bulging based on the proposed fracture criterion are recommended. Designers can adopt the most appropriate forming path according to the requirements of each specific case.

Keywords: Superplastic forming; Instability; Strain concentration; Unstable plastic flow; Stability criterion; Flow localization factor; Finite element model; Fracture criterion

1. Introduction

The most common form of superplastic forming (SPF) is blow-forming (bulging). The forming pressure is often regulated by the well-developed constant strain rate control. That is the strain rate corresponding to the highest strain rate sensitivity is maintained throughout the forming process. However, this value of the strain rate is usually very small. Consequently, the forming time is often excessively long.

Since SPF is a slow process, there is a strong incentive to increase the efficiency of production. Forming the workpiece with higher pressures, however, can lead to less uniform distribution of wall thickness, thus resulting in a lower quality part. To balance productivity and quality, Ding et al. [1,2] proposed variable strain rate paths that ensured a stable deformation for bulging of Ti–6Al–4V sheets. It was shown by finite element simulations that a reduction in the forming time could be achieved compared to the conventional constant strain rate control method, while the uniformity of wall thickness distribution was hardly affected.

In their studies, Ding et al. control the deformation along the limit of stability. However, superplastic materials possess excellent necking resistance and can undergo large amounts of deformation even after the onset of instability. Therefore, further improvement in productivity of SPF can be made. To further improve the productivity of SPF, while at the same time maintain the required thickness distribution and avoid fracturing during the forming process, analysis of flow localization process during superplastic deformation and a fracture criterion are required.

For superplastic materials that are not sensitive to cavity growth, fracturing is dominated by the localization process of unstable plastic flow [3]. We proposed in our previous study [4] a flow localization factor (FLF), which enables quantitative description of the flow localization process for both uniaxial tension and biaxial stretching. In this paper, a fracture criterion for super-

* Corresponding author. Tel.: +886-2-2362-2191; fax: +886-2-2363-1755.

E-mail addresses: r1852203@w2.me.ntu.edu.tw (L.C. Chung), jhcheng@w3.me.ntu.edu.tw (J.-H. Cheng).

0921-5093/02/$ - see front matter
PII: S0921-5093(01)01818-4

plastic materials that are not sensitive to cavity growth is proposed in terms of the FLF. The proposed fracture criterion and the analysis of flow localization process are then applied to design SPF processes for the achievement of both productivity and quality (uniformity).

2. Analysis for flow localization

2.1. Flow localization factor

The FLF, which enables quantitative description of flow localization, has been derived in our previous work [4], and a brief review will be presented here.

For biaxial stretching, the deformation is unstable if [1]

$$\frac{\delta \dot{A}}{\delta A} > 0 \tag{1}$$

where A is the cross-sectional area, and the operator δ signifies a variation between the nominal area and a local nonuniformity. Since $\dot{A} < 0$ in a stretching process, the above equation can be expressed as

$$-\frac{A}{\dot{A}}\frac{\delta \dot{A}}{\delta A} > 0 \tag{2}$$

or

$$\frac{-\delta \ln \dot{A}}{\delta \ln A} > 0 \tag{3}$$

which characterizes the degree of flow localization, and is defined as the FLF. It can be shown that

$$\frac{-\delta \ln \dot{A}}{\delta \ln A} = -\frac{A}{\dot{A}}\frac{\delta \dot{A}}{\delta A} = \frac{\bar{\sigma} - a(\partial \bar{\sigma}/\partial \bar{\varepsilon})}{\dot{\bar{\varepsilon}}(\partial \bar{\sigma}/\partial \dot{\bar{\varepsilon}})} - 1$$

$$= \frac{1 - a(1/\bar{\sigma})(\partial \bar{\sigma}/\partial \bar{\varepsilon})}{(\dot{\bar{\varepsilon}}/\bar{\sigma})(\partial \bar{\sigma}/\partial \dot{\bar{\varepsilon}})} - 1 \tag{4}$$

where

$$a = \sqrt{\frac{4}{3}(1 + \rho + \rho^2)} \quad \text{with} \quad \rho = \frac{\dot{\varepsilon}_2}{\dot{\varepsilon}_1} \tag{5}$$

which is a factor governing principal strain rate ratio. Defining the strain hardening coefficient (γ) and the strain rate sensitivity (m) to be

$$\gamma = \frac{1}{\bar{\sigma}}\left(\frac{\partial \bar{\sigma}}{\partial \bar{\varepsilon}}\right), \quad m = \frac{\dot{\bar{\varepsilon}}}{\bar{\sigma}}\left(\frac{\partial \bar{\sigma}}{\partial \dot{\bar{\varepsilon}}}\right) \tag{6}$$

the FLF defined by Eq. (4) for biaxial stretching is expressed as

$$\xi_{\mathrm{II}} = \frac{1 - a\gamma}{m} - 1 \tag{7}$$

where the subscript II indicates 'biaxial.' Under uniaxial tension, $\rho = -0.5$ and $a = 1$, and ξ_{II} reduces to ξ_{I}

$$\xi_{\mathrm{I}} = \frac{1 - \gamma}{m} - 1 \tag{8}$$

where the subscript I indicates 'uniaxial.' This form is similar to that proposed by Cáceres and Wilkinson [5].

The physical meaning of the FLF is the degree of flow localization. When $\gamma \geqslant 1$, a neck does not grow [6]. This condition corresponds to $\xi_{\mathrm{I}} \leqslant -1$. On the other hand, when $\xi_{\mathrm{I}} > -1$, a neck starts to grow, with higher ξ_{I} leading to more severe flow localization and the condition $\xi_{\mathrm{I}} \leqslant 0$ corresponding to Hart's stability criterion [7], $\gamma + m \geqslant 1$. It should be noted that the FLF applies to both uniaxial tension and biaxial stretching conditions, while the parameters proposed in other works [5,6] to describe flow localization are only valid for uniaxial tension.

Before we state the fracture criterion, a series of experiments and finite element simulations are performed to gain some confidence on analysis accuracy and to reveal physical insights of the FLF.

2.2. Experimental method

Since the Ti–6Al–4V alloy is not sensitive to cavity growth and the fracture mode is dominated by unstable plastic flow [8], this material was used in this research to study the relation between the FLF and the forming limits of superplastic bulging. We designed a series of experiments of superplastic fracture bulging by placing a 2.0-mm thick Ti–6Al–4V sheet over a cone-shaped die, and high purity argon gas was blown over one side of the sheet at 900 °C until fracturing occurs. The fracture time was then measured. A schematic diagram for superplastic bulging of a cone is shown in Fig. 1.

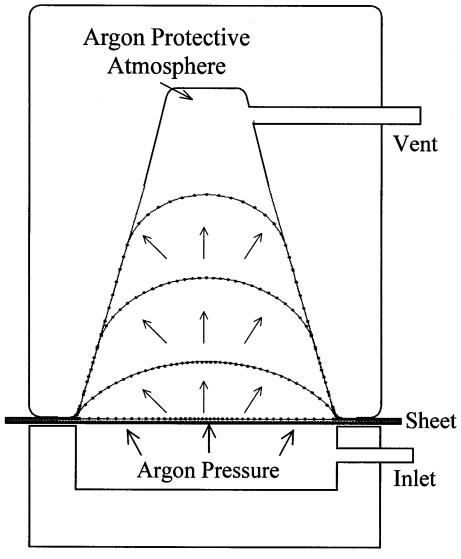

Fig. 1. Schematic diagram for superplastic bulging of a cone.

Table 1
Fracture time of Ti–6Al–4V sheets bulged at 900 °C

Forming pressure (MPa)	2.94	2.548	2.254	1.96	Step-down	Step-up
Fracture time (s)	591	748	883	1133	858	838

Bulgings with constant pressures of 2.94, 2.548, 2.254 and 1.96 MPa have been accomplished in the previous work, and the experimental details are given in Ref. [4]. The results are shown in the first five columns in Table 1.

In the present work, two other pressure profiles were also applied in the bulging experimentation. One is the step-down profile, and the other is the step-up profile, as shown in Fig. 2. The step-down profile describes a pressure profile that remains at 2.94 MPa initially, then drops linearly to 1.96 MPa from 320 to 360 s, and then maintains the final value until the formed part fractures. The step-up profile describes a pressure profile that is held at 1.96 MPa initially, then is raised linearly to 2.94 MPa from 500 to 540 s, and then maintains the final value until the formed part fractures.

2.3. Finite element simulation

A commercial finite-element package, ABAQUS, was used to perform the modeling and analysis for the experiments. The die is considered rigid, and the sheet is modeled by two-node linear axisymmetric membrane elements. The material behavior is modeled by the constitutive relation $\bar{\sigma} = K\dot{\bar{\varepsilon}}^m\bar{\varepsilon}^n$, in which m and n are functions of strain rate. With this relation, $\gamma = n/\bar{\varepsilon}$. This constitutive relation indicates that both the strain hardening and strain rate hardening effects are considered. Details of how the finite element model was established are also given in Ref. [4], where a verification showed that this model produced simulation results in good agreement with experiments. The FLF at fracture points is also computed by means of the finite element simulation.

2.4. Results and discussions

The fracture time for the bulging experiments described in Section 2.2 is shown in Table 1 (the data presented are average values of several experiments).

Fig. 3 shows the computed curves of the FLF at the fracture points (the summits of the superplastically formed cones) versus forming time during constant pressure bulging. From the figure, as discussed in Ref. [4], the localization process during constant pressure bulging can be divided into three stages, which are (1) the developing period of initial localized flow, (2) the steady stage of strain concentration, and (3) the accelerating stage of strain concentration. The second stage

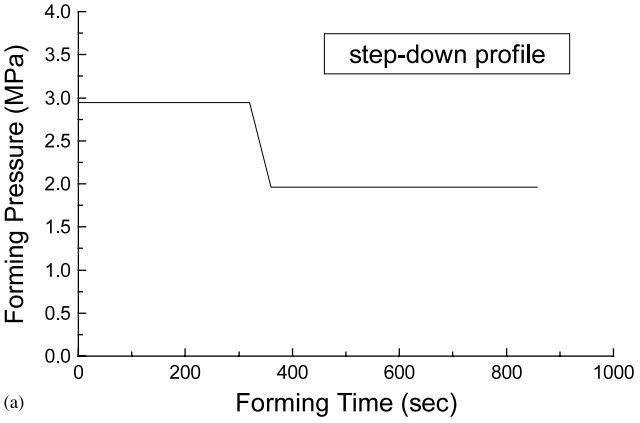

Fig. 2. Step-down and step-up pressure profiles.

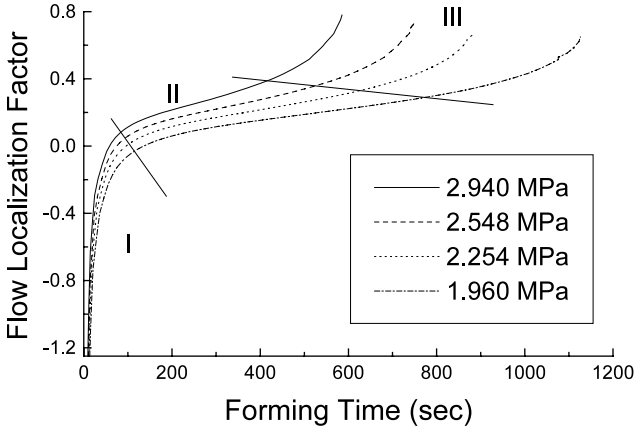

Fig. 3. FLF versus forming time during constant pressure bulging.

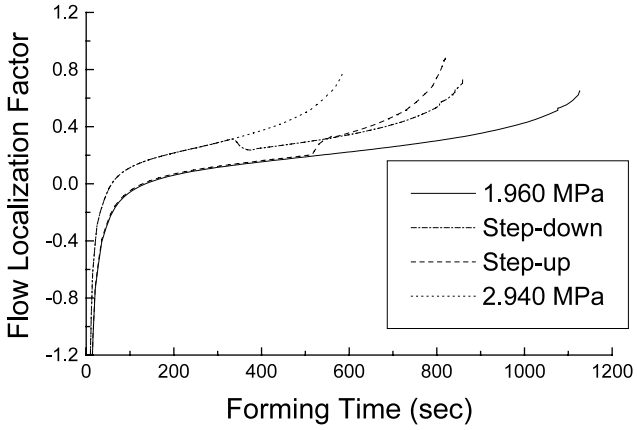

Fig. 4. FLF versus forming time for various pressure profiles.

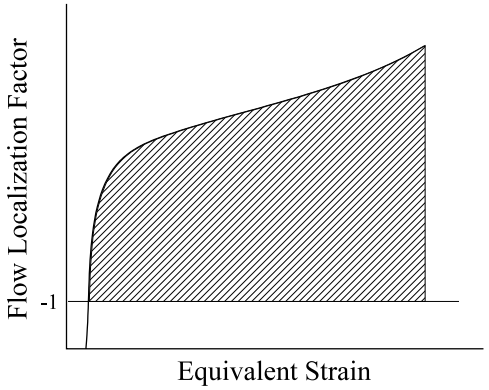

Fig. 5. Definition of C.

takes the greatest part of the forming time, and strain concentration is apparent throughout the third stage, until the end of the forming process, when fracturing occurs.

The curves of the FLF at the fracture points versus forming time for bulgings with step-down and step-up pressure profiles are shown in Fig. 4, where the curves for bulgings with constant pressures of 1.96 and 2.94 MPa are also shown for comparison. For bulgings with step pressure profiles, the FLF drops or rises suddenly when the pressure drops or rises, indicating that the degree of flow localization changes rapidly during those periods.

The above characteristics can be explained by the fact that the FLF represents the degree of flow localization at an 'instant' of time. When the forming pressure changes suddenly, the tendency of the degree of flow localization changes at that instant. Therefore, the value of the FLF drops or rises at that time. In the case of step-down pressure profile, when the pressure drops, the thickness of the formed part is still thinning. That means that the material is still approaching its forming limit, and yet the value of the FLF decreases. Consequently, the FLF cannot be directly used to predict the forming limits.

For superplastic materials that are not sensitive to cavity growth, fracturing can be viewed as the result when the flow localization accumulated at a material point during a forming process reaches a critical value. Since the FLF represents the degree of flow localization at an 'instant,' a quantity defined properly by integrating the FLF can stands for the flow localization accumulated throughout the whole forming process, and thus can be regarded as the index of fracturing. This concept is used to propose a fracture criterion in the next section.

3. Fracture criterion and verifications

3.1. Fracture criterion

The combination of two processes, localization of unstable plastic flow and evolution of internal cavities, controls the fracture mode of superplastic metals [8]. It has been shown by Zhou et al. [3] that for superplastic materials that are not sensitive to cavity growth, the fracture mode is dominated by unstable plastic flow, and the localization process of unstable plastic flow controls the amounts of useful deformation that the material can endure prior to failure. A number of studies have predicted the limit strains in superplastic tensile tests [7,9–15], but few have worked on the forming limits of superplastic bulging (under biaxial stretching conditions). In this section, a fracture criterion, which is valid for both uniaxial tension and biaxial stretching, is proposed for materials that are not sensitive to cavity growth.

As discussed in Section 2.1, when the FLF is greater than -1, a neck starts to grow. The duration of neck growth is the stage of flow localization. Therefore, the index for fracture can be defined by integrating the FLF from -1 until the material cracks, which is the area enclosed by the shaded area shown in Fig. 5, i.e. the area between the 'ξ_{II} versus $\bar{\varepsilon}$' curve and the line $\xi_{II} = -1$. In order to avoid integrating from -1, we can re-express the fracture index as

$$C = \int_0^{\bar{\varepsilon}} J \, \mathrm{d}\bar{\varepsilon} \tag{9}$$

where

$$J = \begin{cases} \xi_{II} + 1 & \text{if } \xi_{II} + 1 > 0 \\ 0 & \text{if } \xi_{II} + 1 \leqslant 0 \end{cases} \tag{10}$$

When fracture occurs, C reaches a critical value C_{cr}, i.e.

$$\int_0^{\bar{\varepsilon}_f} J \, \mathrm{d}\bar{\varepsilon} = C_{cr} \tag{11}$$

where $\bar{\varepsilon}_f$ is the fracture strain.

Eq. (11) is the fracture criterion proposed for this study. Under uniaxial tension, ξ_{II} reduces to ξ_I, so this criterion applies to both uniaxial tension and biaxial stretching.

3.2. Verifications

It is assumed that C_{cr} is a material property, that is, it is only a function of material ingredients, grain size, and temperature, and does not vary for different pressure profiles, sheet thickness, and die geometry. In this work, the material used is of the same ingredients and grain size, and the forming temperature is the same for all cases. Therefore, C_{cr} can be viewed as a constant.

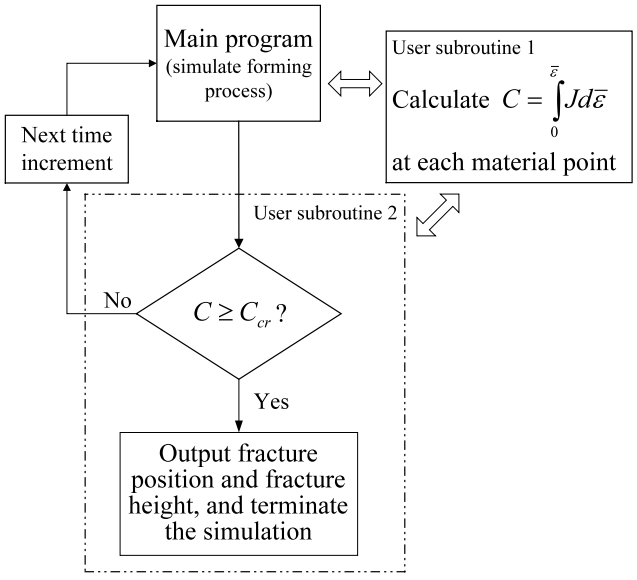

Fig. 6. Implementation of fracture criterion in finite element program.

Table 2
C_{cr} for Ti–6Al–4V sheets at 900 °C

Forming pressure (MPa)	2.94	2.548	2.254	1.96
Fracture time (s)	591	748	883	1133
C_{cr}	2.872	2.951	2.894	3.040
Average C_{cr}	2.939	2.939	2.939	2.939

Table 3
Prediction of forming limits for step pressure profiles

Pressure profile	Step-down	Step-up
Fracture height		
Prediction (mm)	46.5	44.6
Exp. (mm)	48.0	47.5
Err%	−3.13	−6.11

The procedure for verifying the assumption is as follows.

1. Simple bulging experiments are performed to measure the fracture time.
2. The simple experiments are simulated by finite element models in which the forming times are set the same as the fracture time measured. Thus, the value of C_{cr} can be calculated by the finite element simulation.
3. Finite element models are performed to simulate bulgings under different conditions and predict the fracture heights and fracture positions by the value of C_{cr} obtained in the previous step.
4. Experiments under those conditions in step 3 are performed to obtain fracture heights and fracture positions, which are compared with those predicted in step 3 to verify the assumption for the fracture criterion proposed.

How the fracture criterion is implemented in the finite element program is shown in Fig. 6. The whole model includes a main part of the program and two user subroutines. The main program simulates the forming process, and subroutine 1 calculates the value of C at each material point. The C values are then passed into subroutine 2 to check if the C value at any material point exceeds C_{cr}. If any C value exceeds C_{cr}, subroutine 2 will output the fracture position and fracture height, and terminate the simulation. If every C value is less than C_{cr}, the main program will run the next time increment, until fracture occurs.

3.2.1. Obtaining C_{cr}

Simple experiments of constant pressure bulgings described in Section 2.2 are simulated by finite element models with forming time set equal to the fracture time obtained from experiments. The fracture point is at the summit of the blow-formed cone. Therefore, C_{cr} is calculated at the point. The results are shown in Table 2, with the average value of C_{cr} being 2.939. Since it is assumed that C_{cr} does not vary for different pressure profiles, sheet thickness, and die geometry, C_{cr} obtained in this section will be used in the following sections to predict forming limits under different conditions.

3.2.2. Different pressure profiles

Finite element models are performed to simulate the bulgings with step-down and step-up pressure profiles described in Section 2.2, and the values of C (Eq. (9)) are calculated at every material point. If the C value at any material point exceeds C_{cr}, the simulation stops and outputs the position of that point and the forming height at that instant.

All the predicted fracture positions and experimental fracture positions are at the summit of the formed parts. The predicted and experimental fracture heights are summarized in Table 3. The results show that C_{cr}

Table 4
Prediction of forming limits for sheet with 1.0 mm thickness

Forming pressure (MPa)	2.45	1.96	1.47
Fracture height			
Prediction (mm)	37.5	40.5	44.1
Exp. (mm)	36	37.5	42.0
Err%	4.17	8.0	5.0

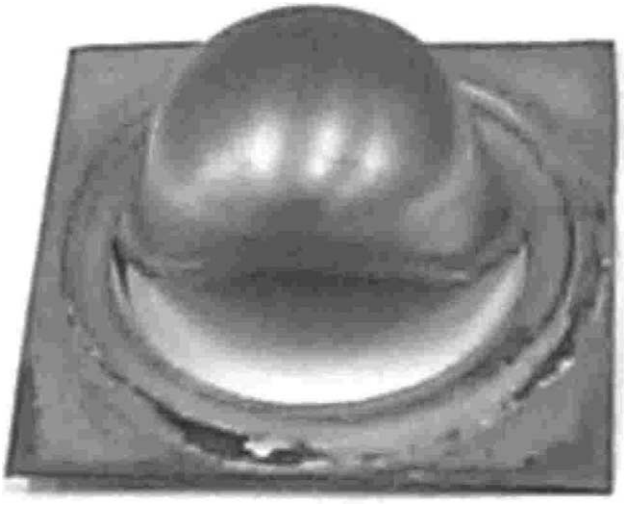

Fig. 7. Fracture at DER.

obtained in Section 3.2.1 can be used to predict the forming limits under these forming conditions.

3.2.3. Different sheet thickness

Constant pressure bulgings with sheets of 1.0 mm thickness are simulated with forming pressures being 2.45, 1.96 and 1.47 MPa, respectively. The die shape, sheet material, and forming temperature remain the same as described in Section 2.2.

The predicted fracture positions coincide with the experimental ones—the summit of the formed parts. Table 4 summarizes the predicted and the experimental fracture heights. The predicted fracture heights are in good agreement with the experimental ones, indicating that the forming limits under these forming conditions are successfully predicted by using C_{cr} obtained in Section 3.2.1.

3.2.4. Fractures at die entry region

During the heating process, the upper and lower dies clamp the softened sheet at high temperature. As a result, the sheet around the die entry region (DER) becomes thinner before the forming pressure is applied. For bulging as described in Section 2.2, lower forming pressures cause faster thinning at the summit of the workpiece than at the DER, leading to fracture at the summit. On the other hand, higher pressures result in faster thinning at the DER, leading to fracture at that position (Fig. 7).

Certainly, finite element models can simulate the thinning phenomenon at the DER before the forming pressure is applied. However, the measured values were directly included in the finite element models. The thinning phenomenon measured for initial sheet thickness of 2.0 and 1.0 mm is shown in Table 5. Simulation results of fracture bulging coincide with the experimental ones and are shown in Table 6, indicating that using C_{cr} obtained in Section 3.2.1 to predict fracture at the DER is successful.

Table 6
Fracture positions for lower and higher pressures (simulation and experiments)

Initial sheet thickness (mm)	2.0	2.0	1.0	1.0
Forming pressure (MPa)	2.94	3.92	2.45	2.94
Fracture position	Summit	DER	Summit	DER

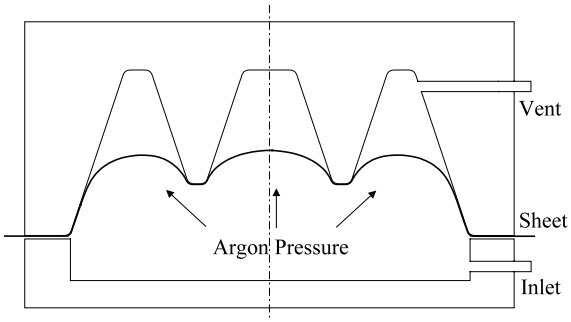

Fig. 8. Schematic diagram for superplastic bulging into a complex die.

3.2.5. Different die shape

A more complex die was designed for the verification of different die shape. The die is axisymmetric and a schematic diagram for superplastic bulging into the die is shown in Fig. 8. A finite element model similar to the one described in Section 2.3 was established to simulate bulging with constant pressure of 1.96 MPa. The sheet thickness is 2.0 mm and the forming temperature is 900 °C.

Table 5
Thinning at DER

Initial sheet thickness (mm)	2.0	2.0	2.0	2.0	1.0	1.0	1.0	1.0
Thickness around DER (mm)	1.27	1.29	1.44	1.53	0.67	0.63	0.78	0.64
Average (mm)	1.38	1.38	1.38	1.38	0.68	0.68	0.68	0.68

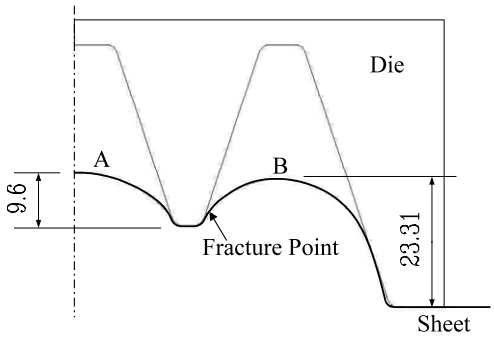

Fig. 9. Predicted fracture position and heights for bulging with complex die.

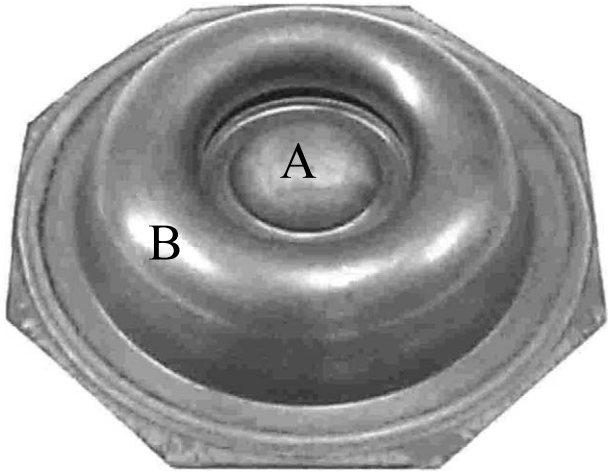

Fig. 10. Experimental result of bulging into complex die.

Table 7
Prediction of forming limit for bulging into a complex die

Part	A	B
Fracture height		
Prediction (mm)	9.6	23.31
Exp. (mm)	10.2	24.4
Err%	−6.25	−4.68

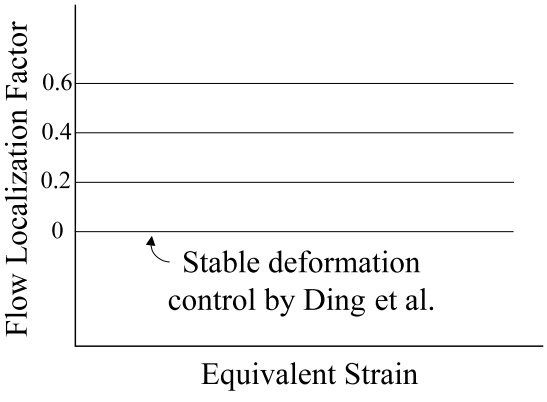

Fig. 11. Constant FLF control.

Fig. 9 shows the predicted result that the sheet is fractured into parts A and B, with the fracture heights being 9.6 and 23.31 mm, respectively. The experimental result is shown in Fig. 10, in which the fracture position coincides with the predicted one. Table 7 shows that the predicted fracture heights of parts A and B are in good agreement with the experimental ones.

4. Forming pressure design

Two factors are usually given serious consideration in practical superplastic bulging. One is the duration of the forming time. Reduced forming time leads to improved productivity. The other is the uniformity of wall thickness, which affects the quality of formed parts. However, it is difficult to achieve both of these goals at the same time [2]. More uniform distribution of wall thickness requires longer forming time, while reducing forming time by increasing forming pressure causes less uniform thickness distribution or even fracturing before the parts are completely formed.

In order that designers can select the most appropriate pressure profile according to the requirements of each particular case, design guidelines are proposed in this section. Finite element models in this section were established including the fracture criterion to ensure that the formed parts would not fracture under the forming conditions in this section. The processes simulated are blow-forming sheets into a cone-shaped die and are the same as described in Section 2.2 except that the sheet thickness is 1.0 mm and the pressure control methods are different.

4.1. Pressure controls

Variable strain rate paths that ensured a stable deformation (Hart's definition) were obtained by Ding et al. for superplastic blow-forming [1,2]. A reduction in forming time was achieved with almost no loss of uniformity in the thickness distribution compared with the conventional constant strain rate control method.

Controlling the deformation along the limit of stability is equivalent to control the FLF at 0. Since superplastic materials possess excellent necking resistance, controlling FLF at higher values can further reduce the forming time without fracturing. Therefore, we proposed a constant FLF control approach, which is to control the FLF (instead of the maximum strain rate) at a given value and is shown in Fig. 11, with the stable deformation control proposed by Ding et al. being a special case. Bulging controlled by conventional constant strain rate control is also examined for comparison.

Finite element simulations were performed to control the forming pressure such that the strain rate or the

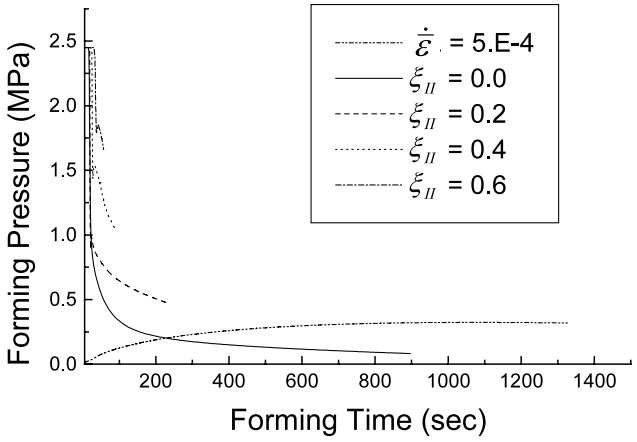

Fig. 12. Pressure profiles for various controls.

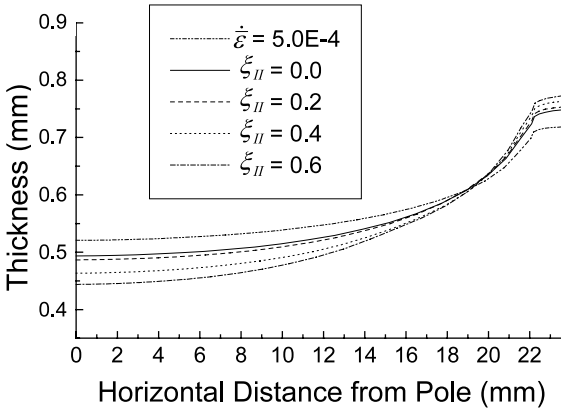

Fig. 13. Thickness distribution for various controls.

FLF were maintained at given values. In the case of constant strain rate control, the strain rate is kept at $\dot{\bar{\varepsilon}} = 5 \times 10^{-4}\ \mathrm{s}^{-1}$, which corresponds to the highest strain rate sensitivity. In the cases of constant FLF control, the FLF is held at 0, 0.2, 0.4, or 0.6. The forming height of all the cases is 20.0 mm, and the pressure profiles obtained from simulations for these cases are shown in Fig. 12, with the upper limit of 2.45 MPa to prevent fracture at the DER.

4.2. Results and discussions

Table 8 shows the forming time for various controls, where the forming path of $\xi_{\mathrm{II}} = 0$ is equivalent to the stable deformation control by Ding et al., and the reduction in forming time is compared with that of the constant strain rate control. Thickness distribution for these controls is shown in Fig. 13. The uniformity of a formed part is defined as the thinnest thickness divided by the thickest thickness, and is also shown in Table 8. It is clear from the table that controlling the forming process with constant strain rate of $5 \times 10^{-4}\ \mathrm{s}^{-1}$ yields the most uniform thickness distribution but the longest forming time. Forming with constant FLF paths results in shorter forming time but less uniform thickness distribution, with higher values of FLF lead to larger amounts of reduction in forming time and some loss of uniformity.

In order to achieve both productivity and quality (defined here as uniformity), one might choose the forming path of $\xi_{\mathrm{II}} = 0.2$, which yields satisfactory thickness distribution and reduces 82% of the forming time compared with the conventional constant strain rate control. The FLF value suggested here, however, may alter from case to case. In practice, designers can adopt the most appropriate forming path in accordance with the requirements of each case. If the best uniformity is needed, the constant strain rate control should be used. Otherwise, if the shortest forming time is required, then the forming path with highest FLF value can be adopted on the premise that the workpiece will not fracture. For instance, if it is required that the forming height is 40.0 mm and the forming time is shortest, finite element simulation shows that the forming path of $\xi_{\mathrm{II}} = 0.6$ results in premature fracture when the forming height is 38.3 mm, and thus the controlled FLF value should be lowered. However, the forming path of $\xi_{\mathrm{II}} = 0.5$ is shown to successfully form the part. The forming time is 317 s, which is the shortest with constant FLF control and is 90% less than that required with the constant strain rate control (Table 9).

Table 9
Forming time needed for a 40.0 mm high part by various controls

Forming path	$\dot{\bar{\varepsilon}} = 5 \times 10^{-4}\ \mathrm{s}^{-1}$	$\xi_{\mathrm{II}} = 0$	$\xi_{\mathrm{II}} = 0.5$
Forming time (s)	3125	2120	317
Reduction in forming time	0	32%	90%

Table 8
Forming time for various controls

Forming path	$\dot{\bar{\varepsilon}} = 5 \times 10^{-4}\ \mathrm{s}^{-1}$	$\xi_{\mathrm{II}} = 0$	$\xi_{\mathrm{II}} = 0.2$	$\xi_{\mathrm{II}} = 0.4$	$\xi_{\mathrm{II}} = 0.6$
Forming time (s)	1328	896	239	91.9	57.2
Reduction in forming time (%)	0	33	82	93	96
Uniformity	0.73	0.67	0.65	0.61	0.58

5. Conclusions

The FLF was proposed in our previous work [4] to quantitatively describe the flow localization process of superplastic materials. Utilizing the FLF, further studies in this paper are concentrated on the forming limits and pressure design of superplastic bulging. From the analysis and experimental results, the followings are concluded.

The FLF stands for the degree of flow localization at an instant.

A fracture criterion for superplastic materials that are not sensitive to cavity growth is proposed in terms of the proper integral form of the FLF.

For superplastic materials that are not sensitive to cavity growth, fracturing can be viewed as the result when the flow localization accumulated at a material point during a forming process reaches a critical value C_{cr}.

C_{cr} is a material property, i.e. it is only a function of material ingredients, grain size, and temperature.

Bulging with higher values of the FLF leads to shorter forming time but less uniform thickness distribution.

Pressure design guidelines for superplastic bulging are proposed. Designers can choose the most proper forming path according to the requirements of each case.

Acknowledgements

This research was sponsored by the National Science Council of the Republic of China.

References

[1] X.D. Ding, H.M. Zbib, C.H. Hamilton, A.E. Bayoumi, J. Eng. Mater. Technol, Trans. ASME. 119 (1997) 26–31.
[2] X.D. Ding, H.M. Zbib, C.H. Hamilton, A.E. Bayoumi, J. Mater. Eng. Perform. 4 (4) (1995) 474–485.
[3] D.-J. Zhou, J. Lian, M. Suery, Mater. Sci. Technol. 4 (1988) 348–353.
[4] L.C. Chung, J.H. Cheng, Mat. Sci. Eng. A308/1–2 (2001) 153–160.
[5] C.H. Cáceres, D.S. Wilkinson, Acta Metall. 32 (3) (1984) 415–422.
[6] E. Sato, K. Kuribayashi, ISIJ. Int. 33 (8) (1993) 825–832.
[7] E.W. Hart, Acta Metall. 15 (1967) 351–355.
[8] J. Pilling, N. Ridley, Cavitation and fracture, in: Superplasticity in Crystalline Solids, Camelot Press/The Institute of Metals, Southampton, 1989, pp. 102–158.
[9] W.B. Morrison, Trans. Met. Soc. AIME 242 (1968) 2221.
[10] F.A. Nichols, Acta Metall. 28 (1980) 663–673.
[11] K. Marciniak, K. Kuczynski, T. Pokora, Int. J. Mech. Sci. 15 (1973) 789.
[12] A.K. Ghosh, R.A. Ayres, Metall. Trans. 7A (1976) 1589–1591.
[13] J.W. Hutchinson, K.W. Neale, Acta Metall. 25 (1977) 839–846.
[14] U.F. Kocks, The initiation and development of deformation inhomogeneities in superplastic materials, in: Superplastic Forming of Structural Alloys, TMS/AIME, San Diego, 1982, pp. 41–55.
[15] A. Arieli, B.J. Maclean, A.K. Mukherjee, Res. Mech. 6 (1983) 131–159.